Docket No. UTAD 0001 PATENT APPLICATION

PARAMAGNETIC METAL ION-BASED MACROCYLIC MAGNETIZATION TRANSFER CONTRAST AGENTS AND METHOD OF USE

Inventors: A. Dean Sherry
6934 Spanky Branch Drive
Dallas, Texas 75248

Shanrong Zhang
5200 Meadowcreek Drive, #1058
Dallas, Texas 75248

Kuangcong Wu
2524 Cima Hill Drive
Plano, Texas 75023

Assignee: Board of Regents,
The University of Texas System
207 West 7th Street, Suite 820
Austin, Texas 78701

Hitt Gaines & Boisbrun, P.C.
P.O. Box 832570
Richardson, Texas 75083
(972) 480-8800

PARAMAGNETIC METAL ION-BASED MACROCYLIC MAGNETIZATION TRANSFER CONTRAST AGENTS AND METHOD OF USE

CROSS-REFERENCE TO PROVISIONAL APPLICATION

[0001] This application claims the benefit of U.S. Provisional Application 60/252,269 entitled, "LANTHANIDE-BASED MAGNETIZATION TRANSFER (MT) CONTRAST AGENTS FOR MAGNETIC RESONANCE IMAGING (MRI)," to A. Dean Sherry, Shanrong Zhang and Kuangcong Wu, filed on November 20, 2000, which is commonly assigned with the present invention and incorporated herein by reference as if reproduced herein in its entirety.

TECHNICAL FIELD OF THE INVENTION

[0002] The present invention is directed to contrast agents and methods of using contrast agents for altering the magnetic resonance signal of samples, and more particularly, to paramagnetic metal ion-macrocylic complexes as contrast agents and methods of using such agents for producing image contrast based on a magnetization transfer mechanism.

BACKGROUND OF THE INVENTION

[0003] Contrast agents (CAs) are widely used to enhance magnetic resonance imaging (MRI) contrast. The administration of Extrinsic CAs, such as gadolinium (Gd) containing CAs, are thought to achieve contrast by the paramagnetic relaxation effect of a metal-ion to shorten the bulk water relaxation time via rapid exchange of the metal ion's inner-sphere water molecules with bulk solvent. The ability to turn CAs on or off raises the possibility of using such CAs to measure changes in physiological status of tissue samples. For example some CAs exclude Gd from the inner sphere while inactive, and then on activation expose bulk water to a rapidly exchanging water site on the Gd. However, the utility of such CAs in living subjects may be limited by toxicity and undesirable spin-spin lattice relaxation time ($T2^*$) effects. In addition, CAs having a slow rate of water exchange are disfavored because this hampers the metal-ion's ability to shorten the bulk water relaxation time and thus enhance contrast.

[0004] Chemical exchange saturation transfer (CEST) is an alternative technique to enhance MRI contrast. Contrary to the above described CAs, CEST favors CAs having a slow rate of water exchange. For example, intrinsic metabolites with slowly exchangeable NH or OH sites may be saturated to produce a direct

intensity decrease in the bulk water signal by Magnetization Transfer (MT). It may also be possible to develop MT-based CA that turn on an off in response to a physiologic parameter, such as pH, if the exchange rate of the NH or OH sites are sensitive to changes in that parameter. However, because the chemical shifts of such diamagnetic NH and OH groups in intrinsic metabolites are typically within 5 ppm of bulk water, it can be difficult to avoid off-resonance saturation of bulk water or tightly protein-bound water in tissue samples. Extrinsic CAs may similarly enhance image contrast by MT. Such CAs, however, rely on the chemical exchange of NH or OH functional groups covalently bonded to the CA and close to the resonance frequency of bulk water.

[0005] Accordingly, what is needed is an improved MT-based CA that is amenable to discriminating and reporting on the changing metabolic status of a target sample in contrast to its surroundings.

SUMMARY OF THE INVENTION

[0006] To address the deficiencies of the prior art, the present invention, in one embodiment, provides a contrast agent comprising: a tetraazacyclododecane ligand having a general formula as follows:

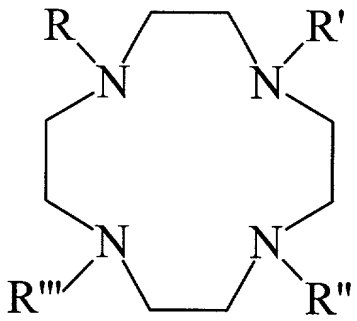

wherein pendent arms R, R′, R′′ and R′′′ are amides having a general formula: $-CR_1H-CO-NH-CH_2-R_2$, wherein R_1 includes organic substituents and R_2 is not hydrogen; and a paramagnetic metal ion coordinated to the tetraazacyclododecane ligand.

[0007] In another embodiment, the present invention provides a method of using a magnetic resonance (MR) contrast agent, comprising: subjecting a contrast agent contained within a sample to a radio frequency pulse wherein the contrast agent is a tetraazacyclododecane ligand having the above described general formula, wherein pendent arms R, R′, R′′ and R′′′ comprise organic substituents and the tetraazacyclododecane ligand further includes a paramagnetic metal ion coordinated to the tetraazacyclododecane ligand and a water molecule associated with the tetraazacyclododecane ligand; and obtaining a

magnetization transfer signal by applying a radio frequency pulse at a resonance frequency of the water molecule.

[0008] Yet another embodiment provides a magnetic resonance system, comprising: a magnetic resonance (MR) contrast agent, wherein the MR agent tetraazacyclododecane ligand has the above described general formula, wherein pendent arms R, R', R'' and R''' comprise organic substituents and the tetraazacyclododecane ligand further includes a paramagnetic metal ion coordinated to the tetraazacyclododecane ligand and a water molecule associated with the tetraazacyclododecane ligand, wherein the MR contrast agent produces a magnetization transfer signal when subjected to a radio frequency pulse; and a magnetic resonance apparatus.

[0009] The foregoing has outlined, preferred and alternative features of the present invention so that those skilled in the art may better understand the detailed description of the invention that follows. Additional features of the invention will be described hereinafter that form the subject of the claims of the invention. Those skilled in the art should appreciate that they can readily use the disclosed conception and specific embodiment as a basis for designing or modifying other structures for carrying out the same purposes of the present invention. Those skilled in the art should also realize that such equivalent constructions do not depart from the spirit and scope of the invention.

BRIEF DESCRIPTION OF THE DRAWINGS

[0010] For a more complete understanding of the invention, reference is now made to the following descriptions taken in conjunction with the accompanying drawing, in which:

[0011] FIGURE 1 illustrates a method of using a magnetic resonance contrast agent according to the present invention;

[0012] FIGURE 2 illustrates a magnetic resonance system according to the present invention;

[0013] FIGURE 3 illustrates the dependence of τ_M^{298} on the radius of the central lanthanide ion for a series of lanthanide ion (Ln^{3+}) complexes of the present invention;

[0014] FIGURE 4 illustrates an exemplary ^1H NMR spectrum of the $Eu(\mathbf{1})^{3+}$ complex produced according to the present invention in the absence of a saturating pulse, and a MT profile for the complex;

[0015] FIGURE 5 illustrates an exemplary ^1H NMR spectrum of the $Pr(\mathbf{1})^{3+}$ complex produced according to the present invention in the absence of a saturating pulse, and a MT profile for the complex;

[0016] FIGURE 6 illustrates an exemplary ^1H NMR spectrum of the $Nd(\mathbf{1})^{3+}$ complex produced according to the present invention in the absence of a saturating pulse, and a MT profile for the complex;

[0017] FIGURE 7 illustrates an exemplary ^{1}H NMR spectrum of the $Yb(\mathbf{1})^{3+}$ complex produced according to the present invention in the absence of a saturating pulse, and a MT profile for the complex;

[0018] FIGURE 8 illustrates exemplary MR images of a sample contained the $Eu(\mathbf{1})^{3+}$ complex (inner cylinder) produced according to the present invention in the absence and presence of a saturating pulse at $\pm\Delta\omega$ for bound water, and corresponding difference images;

[0019] FIGURE 9 illustrates exemplary MR images of a sample contained the $Nd(\mathbf{1})^{3+}$ complex (inner cylinder) produced according to the present invention in the absence and presence of a saturating pulse at $\pm\Delta\omega$ for bound water, and corresponding difference images;

[0020] FIGURE 10 illustrates an exemplary relationship of the MT effect versus saturation duration time for the $Eu(\mathbf{1})^{3+}$ complex;

[0021] FIGURE 11 illustrates an exemplary relationship of the MT effect versus saturation power for the $Eu(\mathbf{1})^{3+}$ complex;

[0022] FIGURE 12 illustrates exemplary MR images of a sample containing the $Nd(\mathbf{1})^{3+}$ complex (inner cylinder) produced according to the present invention in the absence and presence of a saturating pulse at $\pm\Delta\omega$ for bound water with different

saturation powers, and corresponding difference images;

[0023] FIGURE 13 illustrates an exemplary ^1H NMR spectrum of the Eu(**2**)$^-$ complex produced according to the present invention in the absence of a saturating pulse;

[0024] FIGURE 14 illustrates an exemplary relationship the pH dependence of the τ_M^{298} for the bound water molecule of the Eu(**2**)$^-$ complex of the present invention;

[0025] FIGURE 15 illustrates an exemplary relationship the pH dependence of the τ_M^{298} for protons associated with the amides in the pendent arms of the Eu(**2**)$^-$ complex of the present invention;

[0026] FIGURE 16 illustrates the pH dependence of the MT effect obtained when saturating the bound water molecule of the Eu(**2**)$^-$ complex of the present invention;

[0027] FIGURE 17 illustrates the relationship between the MT effect obtained when saturating the bound water molecule of the Eu(**2**)$^-$ and the bound water lifetime, τ_M^{298}, or the exchange limiting regime, $\Delta\omega \bullet \tau_M$;

[0028] FIGURE 18 illustrates an exemplary ^1H NMR spectrum of the Eu(**2**)$^-$ complex produced according to the present invention in the absence of a saturating pulse, and a MT profile for the complex produced at three different levels of saturating power;

[0029] FIGURE 19 illustrates exemplary MR images of a sample containing the Eu(**2**)$^-$ complex (inner cylinder) produced according

to the present invention in the absence and presence of a saturating pulse at $\pm\Delta\omega$ for bound water, and corresponding difference images;

[0030] FIGURE 20 illustrates exemplary MR images of a sample containing the Eu(**2**)$^-$ complex (inner cylinder) produced according to the present invention in the absence and presence of a saturating pulse at $\pm\Delta\omega$ for amide protons, and corresponding difference images;

[0031] FIGURE 21 illustrates exemplary MR images of a sample containing the Eu(**2**)$^-$ complex (inner cylinder) produced according to the present invention in the absence and presence of a saturating pulse at $\pm\Delta\omega$ for bound water with different saturation powers, and corresponding difference images;

[0032] FIGURE 22 illustrates exemplary MR images of a sample containing the Eu(**2**)$^-$ complex (inner cylinder) produced according to the present invention in the presence of a saturating pulse at $\pm\Delta\omega$ for amides protons, and corresponding difference images;

[0033] FIGURE 23 illustrates an exemplary ^{1}H NMR spectrum of the Yb(**9**)$^{3+}$ complex produced according to the present invention in the absence of a saturating pulse;

[0034] FIGURE 24 illustrates an exemplary ^{1}H NMR spectra of the Yb(**9**)$^{3+}$ complex produced according to the present invention in the absence of a saturating pulse and at different sample pH;

[0035] FIGURE 25 illustrates an exemplary relationship of the pH dependence of the τ_M^{298} for protons H_a and H_b associated with the amides in the pendent arms of the $Yb(\mathbf{9})^{3+}$ complex of the present invention;

[0036] FIGURE 26 illustrates an exemplary a series of bulk water ^1H NMR spectra obtained for an aqueous solution of $Yb(\mathbf{9})^{3+}$ complex of the present invention obtained while applying a saturating pulse of different duration and centered between the resonance signal of the H_a and H_b associated with the amides in the pendent arms of the complex;

[0037] FIGURE 27 illustrates an exemplary relationship between the MT effect obtained for different concentrations of the $Yb(\mathbf{9})^{3+}$ complex of the present invention;

[0038] FIGURE 28 illustrates an exemplary pH dependence of the MT effect obtained while applying a saturating radio frequency pulse at one or both of the resonance signal of the H_a and H_b associated with the amides in the pendent arms of the $Yb(\mathbf{9})^{3+}$ complex of the present invention;

[0039] FIGURE 29 illustrates an exemplary pH dependence of the MT ratios obtained while applying a saturating radio frequency pulse at one or both of the resonance signal of the H_a and H_b associated with the amides in the pendent arms of the $Yb(\mathbf{9})^{3+}$ complex of the present invention;

[0040] FIGURE 30 illustrates exemplary ^1H NMR spectra and MR

images of a sample containing the $Yb(\mathbf{9})^{3+}$ complex (inner cylinder) produced according to the present invention in the presence of a saturating pulse at $\pm\Delta\omega$ for amides protons, H_a and H_b, associated with the amides in the pendent arms of the complex at two different pHs.

DETAILED DESCRIPTION

[0041] It has been found that water exchange rates for water molecules bound to certain paramagnetic metal ion-macrocylic complexes were sufficiently slow that a separate bound water MR signal, substantially up field or downfield (*e.g.*, about ± 6 ppm or more) from the bulk water MR signal, is observable at room temperature in pure water as solvent. Furthermore, this highly shifted and slowly exchanging bound water molecule may be irradiated to produce magnetization transfer (MT) on bulk water and thereby serve as an effective CA.

[0042] The theory of MT had been known for several decades and was widely used in chemistry and biology. *See e.g.*, Forsen S. & Hoffman R.A., 39 J.CHEM.PHYS. 2892 (1963) and 40 J.CHEM.PHYS. 1189 (1964); Dwek, R. A. NUCLEAR MAGNETIC RESONANCE (N.M.R.) IN BIOCHEMISTRY (Oxford University Press, London, 1973); incorporated herein by reference. Theoretically, the extent of observed MT depends on chemical exchange and relaxation:

$$\frac{M_{on}}{M_{off}} = \left(\frac{1}{1+k_{obs}T_{1sat}}\right) + \left(\frac{k_{obs}T_{1sat}}{1+k_{obs}T_{1sat}}\right)\exp\left[-\frac{\left(1+k_{obs}T_{1sat}\right)}{T_{1sat}}\times t\right] \qquad (1)$$

where M_{on} and M_{off} represent the bulk water signal intensity with or without selective Radio Frequency (RF) irradiation at the exchanging sites, respectively. k_{obs} is the pseudo-first order exchange rate between bulk water and the exchanging protons,

given by the concentration ratio of the exchanging sites relative to water protons divided by the lifetime of the exchange sites, τ_M. T_{1sat} is the spin-lattice relaxation time of the bulk water protons during saturation of the exchangeable protons. For paramagnetic systems, T_{1sat} is no longer a constant, but is rather described by standard theory of paramagnetic relaxation, summarized in equation (2):

$$\frac{1}{T_{1sat}} = r_1[CA] + \frac{1}{T_{1dia}} \qquad (2)$$

Here r_1 is the relaxivity ($mM^{-1}s^{-1}$) of the CA, originating from both inner- and outer-sphere paramagnetic contributions. *See e.g.*, Lauffer R.B., 87 CHEM.REV. 901 (1987), incorporated herein by reference.

[0043] To observe a MT effect, the system ideally should be in an exchange limiting regime, defined as $\Delta\omega \bullet \tau_M \geq 1$. The difference in frequency between the MR frequency of the exchanging sites and the MR frequency of bulk water is defined as $\Delta\omega$. The life-time of the exchanging site is defined as τ_M. One advantage of certain paramagnetic lanthanide macrocylic complexes of the present invention displaying a large $\Delta\omega$ is that faster exchange may take place, because τ_M is short, without approaching the exchange limit. Moreover, because the resonance frequency of the exchangeable water molecule site is distant

from bulk water. For example, $\Delta\omega$ corresponds to about ±6 ppm to about ±500 ppm, and preferably about ± 16 ppm to ± 500 ppm. It is therefore possible to saturate the exchanging site while minimizing off-resonance saturation (*i.e.*, direct saturation) of bulk water, and resulting non-specific, detrimental decreased MR signal intensity.

[0044] The CA of the present invention includes a tetraazacyclododecane ligand having a general formula as follows:

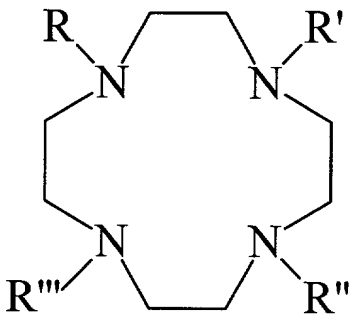

The pendent arms R, R′, R′′ and R′′′ are amides having a general formula: $-CR_1H-CO-NH-CH_2-R_2$, R_1 includes organic substituents and R_2 is not hydrogen.

[0045] The CA may further include a water molecule, referred to as a bound water molecule, as the exchanging group. The bound water molecule is associated with the tetraazacyclododecane ligand and paramagnetic metal ion such that the bound water molecule has a $\Delta\omega \bullet \tau_M \geq 1$. In certain advantageous embodiments of the CA, the bound water has a $\Delta\omega \geq 6$

ppm. In other embodiments of the CA, the bound water molecule has the $\tau_M \geq 1$ μs.

[0046] The CA further comprises a paramagnetic metal ion coordinated to the tetraazacyclododecane ligand. Any paramagnetic metal ion is within the scope of the invention, although certain metal ions of the lanthanide group are preferred. As further detailed in the Experiments below, at magnetic field strengths below 4.7 Tesla (T) the preferred metal ion includes one of Eu^{3+}, Tb^{3+}, Dy^{3+} or Ho^{3+}. At higher field strengths the metal ion may also include Pr^{3+}, Nd^{3+}, Sm^{3+}, Er^{3+} or Tm^{3+}.

[0047] In certain preferred embodiments of this CA, R_2 does not have a proton exchangeable group and is not hydrogen. In other preferred embodiments, R_2 may comprise alkyl groups having 20 carbon atoms or less, cycloalkyl groups having 20 carbon atoms or less, alkyloxy groups having 20 carbon atoms or less, alkyl ethers having 10 oxygen atoms or less and 20 carbon atoms or less, or polyols having 20 carbon atoms or less. R_1 may comprise H, alkyl groups having 20 carbon atoms or less, cycloalkyl groups having 20 carbon atoms or less, alkyloxy groups having 20 carbon atoms or less, alkyl ethers having 10 oxygen atoms or less and 20 carbon atoms or less, or polyols having 20 carbon atoms or less.

[0048] Another embodiment of the present invention is a

method 100 of using a magnetic resonance (MR) contrast agent. As illustrated in FIGURE 1, the method comprises subjecting 110 a contrast agent contained within a sample to a radio frequency (RF) pulse. Here, the contrast agent (CA) is a tetraazacyclododecane ligand having the general formula as presented below:

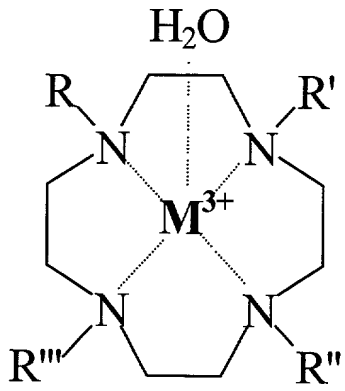

where pendent arms R, R', R'' and R''' comprise organic substituents and the tetraazacyclododecane ligand further includes a paramagnetic metal ion (M^{3+}) coordinated to the tetraazacyclododecane ligand and a water molecule (bound H_2O) associated with the tetraazacyclododecane ligand. The method 100 further comprises obtaining 120 a magnetization transfer (MT) signal by applying 130 a radio frequency pulse at a resonance frequency of the water molecule. In a preferred embodiment of method 100 the water molecule, referred to as a bound water molecule, has a $\Delta\omega \bullet \tau_M \geq 1$. Optionally, method 100 may further include producing a magnetization transfer MR image 140 from the magnetization transfer signal. Method 100 may

optionally further include applying a saturating pulse radio 150 frequency pulse to produce the magnetization transfer signal. Those skilled in the art, however, understand that other means of producing magnetization transfer, for example applying a frequency specific 180° pulse or multi-dimensional NMR techniques, are within the scope of the present invention.

[0049] In one embodiment of method 100 the CA has at least one, and preferably four, pendent arms containing an amide group. Such embodiments of method 100 include obtaining the magnetization transfer signal 120 by applying a radio frequency pulse 160 at a resonance frequency of the protons associated with the amide. As further demonstrated in the Experiments below, the radio frequency pulse may be applied at the resonance frequency of one or all of the exchangeable protons associated with the amide to produce a magnetization transfer signal that is sensitive to pH. The relationship between pH and the magnetization signal may be further be preferably expressed as a ratio of the MT signal obtained while applying the radio frequency pulse one exchangeable amide proton relative to the MT signal obtained while applying the radio frequency pulse to a second or all of the exchangeable amide protons.

[0050] In certain preferred embodiments of method 100, where the pendent arms of the CA each contain an amide group, the pendent arms are identical and have the general formula:

$-CHR_1-CO-NR_2-R_3$, wherein R_1, R_2 and R_3 comprise organic substituents. In one preferred embodiment of this type of CA, the R_1 and R_2 are H, and the R_3 has the general formula: $-(CH_2)_nCOOR_4$ where n = 1-20, and the R_4 is H, a Group IA or IIA metal ions or alkyl group containing from one to twenty carbon atoms. In these preferred embodiments, the paramagnetic metal ion is preferably Tb^{3+}, Dy^{3+} or Ho^{3+} at magnetic field strengths less than 4.7 T, or additionally, Eu^{3+}, Pr^{3+} or Nd^{3+} at higher magnetic field strengths (*i.e.*, 4.7 to 11.75 T). In a second preferred embodiment of the above-described CA, the R_1 and R_2 are H, and the R_3 has the general formula: $-(CH_2)_nP(O)(OR_4OR_5)$ where n = 1-20; R_4 is H, an alkaline earth metal ion of Groups IA or IIA or an alkyl group containing one to twenty carbon atoms; and R_5 also is H, an alkaline earth metal ion of Groups IA or IIA or an alkyl group containing one to twenty carbon atoms. In a third preferred embodiment of the above-described CA, the R_1 and R_2 may be H, and the R_3 has the general formula: $-(CH_2)_nR_4$ where n = 1-20; and R_4 is Pyridine (Py) or Phenol (Ph).

[0051] In another embodiment of method 100, the CA has pendent arms R and R'' that are identical, the pendent arms R' and R''' are identical, and the pendent arms R' and R''' are not equal to the pendent arms R and R''. In one preferred embodiment of the above-described CA, the pendent arms R and R'' have the general formula: $-CHR_1-CO-NH-R_2$; and the pendent arms R' and R'''

have the general formula: $-CHR_3-CO-NH-R_4$ where R_1, R_2, R_3, and R_4 comprise organic substituents, and the R_2 is not equal to the R_4.

[0052] Yet another embodiment of the present invention is a magnetic resonance system 200. As illustrated in FIGURE 2, the system 200 comprises a magnetic resonance (MR) contrast agent (CA) 210, wherein the MR agent contains a tetraazacyclododecane ligand having the same general formula described for method 100. The CA 210 includes pendent arms R, R', R'' and R''' that comprise organic substituents. CA 210 further includes a paramagnetic metal ion coordinated to a water molecule, referred to as a bound water molecule, associated with the tetraazacyclododecane ligand, where the MR contrast agent produces a magnetization transfer signal when subjected to a radio frequency pulse. In certain embodiments of the present invention, the CA includes at least one and up to twenty tetraazacyclododecane ligands. Such ligands may be covalently or noncovalently bonded to a carrier, such as a protein or polymer, comprising a portion of the CA. Collecting several such ligands, and associated metal ions and bound water molecules, allows effective MT contrast to be achieved at lower concentrations of CA. The system 200 further comprises a magnetic resonance apparatus 220. One of ordinary skill in the art understands that the MR apparatus may include all the hardware and software components necessary to produce magnetic

resonance spectra or images.

[0053] The system 200 may further comprise a sample 230 that contains the CA 220 within it. The sample includes living subject including animal, for example human, species, or a portion of fluid or tissue withdrawn from the subject. Alternatively, the sample 230 containing the CA 220 may be an inanimate object, or contain other non-living material. In one preferred embodiment of the MR system 200, the magnetic resonance apparatus 210 produces a magnetization transfer image 240 of the sample 230 from the magnetization transfer signal. Such a system 200 may preferably produce the image by applying the radio frequency pulse at a resonance frequency of the bound water molecule 250. Alternatively the radio frequency signal may be applied at the resonance frequency of protons associated with an amide included in one or more of the pendent arms of the CA 260.

[0054] In certain preferred embodiments of the MR system 200, the magnetic resonance apparatus produces a magnetization transfer difference signal 255 by applying the radio frequency pulse at a $\Delta\omega$ of the bound water molecule, acquiring the magnetization transfer signal and subtracting the signal from a MR signal obtained by applying a radio frequency pulse at $-\Delta\omega$. A difference signal may be produced in analogous fashion, by applying the radio frequency pulse at a $\Delta\omega$ of the protons

associated with amides 265 in the pendent arms of the CA 210 and subtracting the signal from a MR signal obtained by applying a radio frequency pulse at $-\Delta\omega$. In certain embodiments either difference signals 255, 265 may be further processed by the apparatus 220 to produce a difference image. The magnetic resonance system 200 may further include in the apparatus 220 hardware that produces a saturating pulse 270. The saturating pulse is preferably sufficiently frequency specific to saturate only the exchangeable protons, for example the bound water or the protons associated with the amides contained within the pendent arms of the CA 210. The saturating pulse preferably ranges from about 1 to about 3 seconds.

[0055] The CA 210 used in the MR system 200 may include any of the embodiments of CA discussed above in the method 100. However, the exchangeable proton within the CA 210, for example bound water, preferably has a $\Delta\omega \bullet \tau_M \geq 1$. In certain embodiments of the MR system 200, the $\Delta\omega \geq 6$ ppm. In other preferred embodiments of the MR system 200, the $\tau_M \geq 1$ μs.

Experiments

[0056] Examples of CAs prepared according to the present invention are presented below for illustrative purposes and do not limit the scope of the claimed invention. The synthesis of polyazamacrocyles having pendent arms comprising organic

substitutants has been described in: U.S. Patent 5,428,155, to Sherry A.D. and van Westrenen, J.; Kovacs and Sherry, *pH-Controlled Selective Protection of Polyaza Macrocycles*, SYNTHESIS, 761-63, (July 1997); Zhang S., Winter P., Wu. K. & Sherry A.D., *A Novel Europium(III)-Based Contrast Agent*, 123 J.AM.CHEM.SOC. 1517-18 (2001); Zhang S., Wu. K., Biewer M.C., & Sherry A.D. *^{1}H and ^{17}O NMR Detection of a Lanthanide-Bound Water Molecule at Ambient Temperatures in Pure Water*, 40 INORG. CHEM. 4284-90 (2001); which are incorporated herein by reference.

Experiment 1

[0057] A first experiment, examined the life times at 298°K, τ_M^{298}, of water molecules bound to various lanthanide-macrocylic complexes of the present invention, and having the general formula, $Ln(\mathbf{1})^{3+}$, where the four pendent arms R, R', R'' and R''' are all ethyl-acetamidoacetate (*i.e.*, LnDOTA-4AmCE^{3+}), as depicted below:

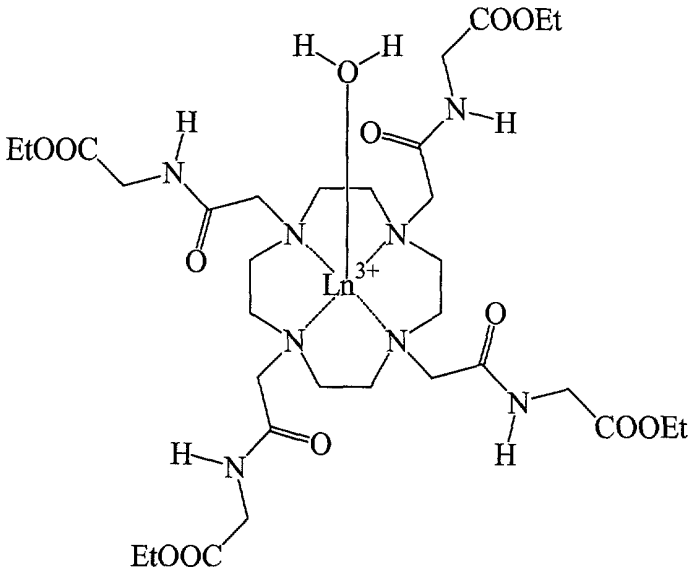

Macrocyclic Complex **1** - $LnDOTA\text{-}4AmCE^{3+}$

[0058] As illustrated in FIGURE 3, τ_M^{298} is strongly dependent on the radius of the central lanthanide ion. The plot shows the τ_M^{298} measured for a series of $Ln(\mathbf{1})^{3+}$ complexes in acetonitrile plus 2-4% water versus the Ln^{3+} ionic radii. Individual τ_M^{298} values were obtained by fitting the temperature dependent ^{17}O NMR bound water line widths according to standard exchange theory. In a separate series of experiments, it was found that τ_M^{298} was about 2-fold shorter when pure water was the solvent. Because the bulk water ^{17}O resonance of Yb(**1**) solution was relatively narrow at all temperatures, no attempt was made to determine τ_M^{298} for this complex based on the ^{17}O NMR line width data from bulk water. However, a fit to the bound-water ^1H NMR line width gave a τ_M^{298} of 5.8 μs for Yb(**1**), consistent with the trend shown in

FIGURE 3. Moreover, ^{1}H NMR line width fitting gave very similar results for those systems for which the bound water is directly observable.

[0059] As further illustrated in Table 1, the proton chemical shifts of bound water in these lanthanide-macrocylic complexes, δ, relative to bulk water, at 0 ppm are generally highly shifted, either more than 6 ppm downfield or upfield (*i.e.*, ± 6 ppm or more), depending upon the properties of the central lanthanide ions. The exchange limit regime, $\Delta\omega \bullet \tau_M$, calculated for different field strengths is also shown in Table 1. At 1.5 Tesla (T), a magnetic field strength presently used by many commercial MRI scanners, the exchange limit regimes, $\Delta\omega \bullet \tau_M$, of Eu(**1**)$^{3+}$, Tb(**1**)$^{3+}$, Dy(**1**)$^{3+}$, and Ho(**1**)$^{3+}$ are all greater than 1. At higher fields, however, such as 4.7 T and 11.75 T, more lanthanide complexes have exchange limit regimes greater than 1, with $\Delta\omega \bullet \tau_M$ increasing as field strength increases. Therefore, favorable MT contrast effects are available for a broad range of lanthanide-macrocylic complexes over a broad range of magnetic field strengths.

TABLE 1

$Ln(1)^{3+}$ Complexes	Observation of bound water	τ_M (μs)	δ (ppm)	$\Delta\omega\bullet\tau_M$		
				11.75 T	4.7 T	1.5 T
Pr^{3+}	Yes	20	-60	3.8	1.5	0.5
Nd^{3+}	Yes	80	-32	8.0	3.2	1.0
Sm^{3+}	Yes	320	-4	4.0	1.6	0.5
Eu^{3+}	Yes	382	50	60.0	24.0	7.7
Tb^{3+}	No	31	-600	58.5	23.4	7.5
Dy^{3+}	No	17	-720	38.5	15.4	4.9
Ho^{3+}	No	19	-360	21.5	8.6	2.8
Er^{3+}	No	9	200	5.7	2.3	0.7
Tm^{3+}	Yes	3	500	4.7	1.9	0.6
Yb^{3+}	Yes	3	200	1.9	0.5	0.2

Experiment 2

[0060] In a second experiment, MT profiles, also known as Z-profiles or CEST profiles, were obtained for lanthanide-macrocylic complexes of the general formula $Ln(1)^{3+}$. FIGUREs 4-7 show representative spectra in the absence of saturation (bulk water peak at 0 ppm truncated to make the bound water peaks more visible) and MT profiles for $Eu(1)^{3+}$, $Pr(1)^{3+}$, $Nd(1)^{3+}$ and $Yb(1)^{3+}$ complexes, respectively, all measured at 4.7 T. All experiments were conducted using aqueous 62.5 mM $Ln(1)^{3+}$ adjusted to neutral

pH and about 22°C, using an saturation duration time of 1 s, RF power of 16 db, and a 2.5 cm surface coil. FIGUREs 4, 5 and 6 illustrate that $Eu(\mathbf{1})^{3+}$, $Pr(\mathbf{1})^{3+}$ and $Nd(\mathbf{1})^{3+}$ all display strong MT properties when a saturating RF pulse is directed at their bound water positions of +50, -45 and -36 ppm, respectively (with bulk water at 0 ppm). Among these three complexes, $Eu(\mathbf{1})^{3+}$, shown in FIGURE 4, had the greatest effect when the saturating pulse was centered at about 50 ppm (arrow): about a 60% decrease in the magnetization of bulk water, M_s, as compared to the magnetization of bulk water in the absence of a saturating pulse, M_o. Importantly, as indicated by a M_s/M_o of about 100%, when the counter-position (*i.e.*, -50 ppm) was saturated, there was no distortion in the bulk water signal. Of course when the saturation pulse is directed to 0 ppm (arrow) there is no signal and therefore M_s/M_o is about 0%. Turning to $Yb(\mathbf{1})^{3+}$, theory suggests that the bound water of $Yb(\mathbf{1})^{3+}$ complex should be at about 200 ppm. Unfortunately, as illustrated in FIGURE 7, no MT effect could be observed for this compound, probably due to its fast exchange, namely an exchange limit regime of less than one ($\Delta\omega \bullet \tau_M = 0.5$).

Experiment 3

[0061] A third series of experiments was performed to examine the ability of lanthanide-macrocylic complexes of the general formula $Ln(\mathbf{1})^{3+}$ to enhance MRI contrast by MT. FIGUREs 8 and

7(21) demonstrate image contrast obtained using aqueous solutions of 62.5 mM Eu(**1**)$^{3+}$ and Nd(**1**)$^{3+}$, respectively. The inner vial contains 62.5 mM Eu(**1**)$^{3+}$ or Nd(**1**)$^{3+}$ at neutral pH, while the outer vial is pure water. T_1-weighted spin-echo images (TR/TE = 500 /18 ms, 256×256 data matrix) were obtained at about 22°C and a field strength of 4.7 T. MT was achieved by applying RF irradiation for 1 s, with a power of 16 db by using a 2.5 cm surface coil. FIGURE 8 shows images obtained with no saturation (left, nosat), saturation at +9800 Hz (middle, Satp) at the resonance frequency of Eu^{3+}-bound water, saturation at -9800 Hz (right, satn), and the corresponding difference images. FIGURE 9 shows analogous images for a phantom with no saturation (left, nosat), saturation at -6400 Hz (middle, Satp) the resonance frequency of Nd^{3+}-bound water, saturation at +6400 (right, satn), and the corresponding difference images. The inner vial contains 62.5 mM Nd(**1**)$^{3+}$ at neutral pH, while the outer vial is pure water. The irradiation duration time was 2 s, with a power of 41 db by using a 2.5 cm surface coil.

[0062] Saturating the bound water at +50 ppm for Eu(**1**)$^{3+}$ (FIGURE 8) and -32 ppm for Nd(**1**)$^{3+}$ (FIGURE 9) resulted in MT to bulk water, thereby providing about an 80% decrease in the bulk water signal in the inner vials without disturbing the imaging intensity of the outer vials. These levels of contrast are much better than expected for diamagnetic CAs where the resonance

signal of the NH or OH group undergoing chemical exchange is only a few ppm away from the resonance signal of bulk water.

Experiment 4

[0063] A fourth experiment was performed under similar conditions as described for Experiments 1-3 to investigate the effect of saturation duration time and power on MT to bulk water. FIGURE 10 shows the relationship of the MT effect versus saturation duration time for the Eu(**1**)$^{3+}$ complex. The theoretical relationship expressed in Equation (1) was fit to this data. The fits reveal that a saturation duration time of one second is sufficient to produce maximum MT effects for the Eu(**1**)$^{3+}$ complex. Similar analysis of data collected for Pr(**1**)$^{3+}$ and Nd(**1**)$^{3+}$ complexes revealed that a saturation duration time of about 1 to about 2 s was sufficient for these paramagnetic MT-CAs.

[0064] FIGUREs 11 and 12 show the relationship of MT effects versus saturation power for Eu(**1**)$^{3+}$ and Nd(**1**)$^{3+}$, respectively. Saturation power level is defined as the times the maximum power of 82 db produced by 4.7 T MRI. A saturation duration time of 3 s was used for all experiments conducted on samples containing Eu(**1**)$^{3+}$. As illustrated in FIGURE 12, saturation power levels (satpl) were increased to examine the effect of power on MT image contrast obtained using Nd(**1**)$^{3+}$. The irradiation duration time was 2 s, and imaging parameters included a TR/TE = 500/18 ms and 64×64 data matrix. As illustrated in FIGUREs 11-12,

contrast continuously improved with increasing saturation power. However, a practical limit of 30-50 db was found for these CAs given the MRI scanner used in these experiments. Other considerations, such as heating of biological or other heat sensitive samples, due to RF power deposition may also limit the saturation power applied. The CA of the present invention are stable to temperatures of at least 100°C.

Experiment 5

[0065] A fifth series of experiments was conducted on a lanthanide-macrocylic complex of the present invention, and having the general formula, Eu(**2**)$^-$, where the four pendent arms R, R′, R′′ and R′′′ are all carboxyl-acetamidoacetate, (*i.e.*,LnDOTA-4AmC$^-$) as depicted below:

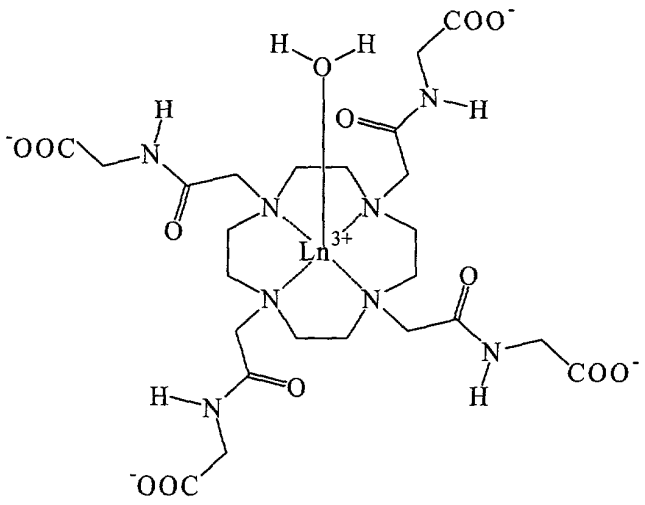

Macrocyclic Complex **2** - LnDOTA-4AmC$^-$

FIGURE 13 shows a 500 MHz 1H NMR spectrum of Eu(**2**)$^-$ complex in an aqueous solution adjusted to pH 7.4 and 25°C. Two sites in the complex (denoted by the symbols *) are chemically exchangeable with bulk water (denoted by the symbol ✧): one is from Eu^{3+}-bound water at about 57 ppm, and another is from four equivalent amide protons on the pendent arms at about -6 ppm.

Experiment 6

[0066] In a sixth series of experiments, the pH dependence of the bound water (FIGURE 14) and the amide (FIGURE 15) protons lifetimes, τ_M^{298}, were determined by variable temperature ^1H NMR line width fitting. The chemically exchangeable bound water and amide protons have different dependence on pH. For bound water protons, the slowest exchange, *i.e.*, largest τ_M^{298}, takes place at pH 7 (FIGURE 14). Moreover, the pH dependence may be divided into two linear ranges: an acidic range where τ_M^{298} = 68.6*pH - 172.5; and a basic range where τ_M^{298} = -128.2*pH + 1212.6, respectively. For the amide protons, the slowest exchange is at pH 5.5 (FIGURE 15). In addition, the exchange limiting regimes ($\Delta\omega \bullet \tau_M$) calculated from the above data, for the magnetic field strength of 4.7, are all larger than 1, thus indicating that either the bound water or amide protons chemical exchange sites may serve as MT-CAs.

Experiment 7

[0067] In a seventh experiment, MT profiles were obtained for 62.5 mM aqueous solutions of the Eu(**2**)$^-$ lanthanide-macrocylic complex. A saturating RF pulse of 2 s at the resonance frequency of bound water or amide protons, with a power of 41 db, was applied to a 3.5 cm volume coil. FIGURE 16 shows that MT decreases were produced for Eu(**2**)$^-$ by saturating bound water proton at about 57 ppm throughout the pH range of 3 to 9. As illustrated in FIGURE 16, the magnitude of MT decrease has a complex dependence upon pH. The same set of data was plotted versus the bound water lifetime, τ_M^{298}, or the exchange limiting regime, $\Delta\omega \bullet \tau_M$, as shown in FIGURE 17. The largest MT occurs for a $\Delta\omega \bullet \tau_M$ ranging from about 12 to about 17, and optimally about 15. FIGURE 18 further demonstrates that the MT effect continues to increase with the magnitude of saturation power applied, up to the maximum power (satpl = 100; corresponding to 82 db) allowed by the MRI instrumentation used in the experiment.

Experiment 8

[0068] An eighth series of experiments was performed to examine the ability of the Eu(**2**)$^-$ lanthanide-macrocylic complex to enhance MRI contrast by MT. Images and difference images were collected under conditions similar to that described for Experiment 3, using a sample comprising a inner vial of 62.5 mM

Eu(**2**)$^-$ and outer vial of water. FIGUREs 19 and 20 are MT images obtained while saturating either the bound water or amide protons, respectively. These figures show that the MR signal of either chemically exchangeable protons may be saturated individually to provide large MT contrasts. For saturation of amide protons, however, a lower saturation power was preferred to avoid direct saturation of the bulk water MR signal. Importantly, by virtue of its farther distance from the bulk water MR signal, higher levels of saturating power, and therefore greater MT contrast, may be obtained by saturating the bound water proton MR signal than that obtained by saturating the amide protons. This point is further illustrated in Experiment 9.

Experiment 9

[0069] In a ninth series of experiments, analogous to Experiment 4, the effect of saturation power on MT to bulk water using the Eu(**2**)$^-$ lanthanide-macrocylic complex was examined. As illustrated in FIGURE 21, a saturating RF pulse was applied at: a) the resonance frequency of bound-water (*i.e.*, satfreq = +11500 Hz), and b) an equal frequency away from the bulk water signal but opposite to the bound water signal (*i.e.*, satfreq = -11500 Hz). The difference image (series c) is shown below. As saturation power level (satpl) was increased, image contrast continuously improved. In comparison, when the amide protons of

$Eu(2)^-$ were saturated, as illustrated in FIGURE 22, as power levels were increased there are serious imaging distortions, mostly likely due to direct saturation of the bulk water.

Experiment 10

[0070] A tenth experiment was conducted on a lanthanide-macrocylic complex of the present invention, and having the general formula, $Ln(9)^{3+}$, where the four pendent arms R, R', R'' and R''' are all acetamidoacetate (*i.e.*, $LnDOTA\text{-}4Am^{3+}$), as depicted below:

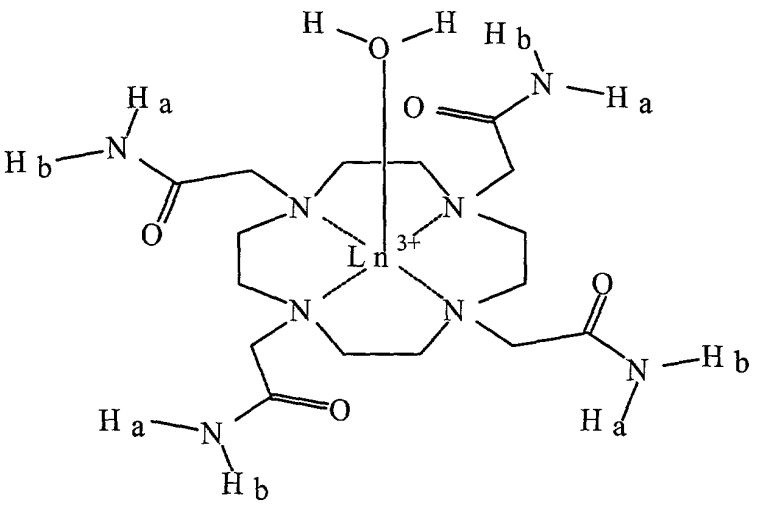

Macrocyclic Complex **9** - $LnDOTA\text{-}4Am^{3+}$

[0071] For certain $Ln(9)^{3+}$ complexes, for example, with Ln equal to Yb or Tm, the bound water molecules are ^1H NMR invisible probably due to the fast exchange between the bound water and the bulk water. However, these complexes are still preferred MT CAs because their ^1H NMR spectra present two sets of amide protons (for example, -14.5 and -17.7 ppm for $Yb(9)^{3+}$, and -42

and -52 ppm for Tm(**9**)$^{3+}$, respectively), which could be saturated to produce MT contrast. FIGURE 23 shows a high resolution ^{1}H NMR spectrum of an aqueous solution containing Yb(**9**)$^{3+}$ adjusted to pH 7.4 and 25°C. Theoretical prediction indicates that a bound water should resonate at about 200 ppm. Unfortunately, the NMR signal was invisible, probably due to its fast exchange with the bulk water. However, the eight exchangeable amide protons present as two resonance peaks with equivalent intensity, at -14.5 (H_a) and -17.7 (H_b) ppm, respectively, are visible.

[0072] As indicated by their linewidths, illustrated in FIGURE 24, the two exchangeable amide sites have different dependences upon pH. As further illustrated in FIGURE 25, H_b exchanges about 1.3 times faster than that of H_a. The exchange limiting regimes, $\Delta\omega \bullet \tau_M$, of both amide protons at magnetic field strength of 7.05 T are much larger that 1, for a broad range of pH values indicating that Ln(**9**)$^{3+}$ complexes in general may be suitable as MT-CAs (TABLE 2). Similar to that discussed above for Ln(**1**)$^{3+}$, either too fast or too slow exchange may produce less MT. For the conditions used to obtain the data presented in Table 2, the maximum MT effect appear to be obtained for Ln(**9**)$^{3+}$ complexes when the exchange limiting regime is about 15.

TABLE 2

pH	τ_M^{298}, ms		$\Delta\omega \bullet \tau_M^{298}$	
	H_a	H_b	H_a	H_b
6.46	5.00	4.00	139.3	133.7
6.76	2.30	1.78	64.1	59.5
7.06	1.21	0.82	33.6	27.2
7.21	0.92	0.72	25.5	24.2
7.43	0.64	0.52	17.9	17.4
7.84	0.57	0.44	15.9	14.7

Experiment 11

[0073] An eleventh series of experiments was conducted to examine the effect of saturation duration on the magnitude of MT obtained using the Yb(**9**)$^{3+}$ complex. FIGURE 26 shows a series of bulk water ^{1}H NMR spectra obtained for an aqueous solution of 5 mM Yb(**9**)$^{3+}$ adjusted to pH 7.4 and 25°C. The upper series of spectra (a) were obtained while applying a saturating pulse of different duration and centered between the resonance signals of the exchangeable amide protons, with a saturating bandwidth of 1500 Hz. The saturating bandwidth was produced using conventional water elimination technique (*i.e.*, a wet1d pulse sequence). *See* Varian User Manual; Varian NMR, Palo Alto, CA; User Guide, VNMR Version 6.1 software, 1997), incorporated

herein by reference. The pulse sequence to produce saturation was modified to include hard loops to shape the pulse train (90° e-burp1, typically repeated from about 0 to about 500 times) with a bandwidth of 1500 Hz (pwwet = 3.0 ms and wetpwr = 28 db). The lower series (b) of spectra, shown inverted to facilitate comparison to series (a), were obtained while applying the same saturating pulse, but on the opposite side and equal distance away from the bulk water MR signal. As the illustrated in FIGURE 26, for a saturating pulse of about 2 s or longer, about a 38% decrease in the bulk water signal was obtained for series (a). In comparison, there was substantially no decrease in the bulk water signal for series (b).

Experiment 12

[0074] A twelfth series of experiments was conducted to examine the effect of the Yb(**9**)$^{3+}$ concentration on the magnitude of MT-based contrast. The concentration dependence of the MT effect obtained for the Yb(**9**)$^{3+}$ complex, measured at pH 7.4 and room temperature, is further illustrated in FIGURE 27. The curve depicts the best fit of a combination of MT theory and paramagnetic theory, presented in Equations 1 and 2, to the experimental data. This shows that substantial MT contrast may be obtained at concentrations similar to CA concentrations in clinical use. The results of FIGURE 27 also illustrate that at a certain concentration of CA, the MT effect is independent of

concentration. While not restricting the scope of the invention to a particular theory, it is believed that the magnitude of MT effect is strongly linked to the paramagnetic properties of the central metallic ions. That is, although the MT effect should be proportional to concentration at all concentrations, when the concentration gets too high, the spin lattice relaxation time of bulk water (T1sat) becomes too short and dominates the MT effect. For example, for the $Yb(\mathbf{9})^{3+}$ complex, at higher concentrations, paramagnetic relaxation effect due to Yb^{3+} predominates at about 20 mM or higher. Under these conditions, there will be no further MT decrease because the saturated MT signal quickly recovers. As such, an optimal concentration is at about 20 mM of the $Yb(\mathbf{9})^{3+}$ complex. Of course, lower concentration of CA may be preferred for other reasons, such as minimizing the dose of CA necessary to administer to a subject. This experiment also suggests that conventional CAs, using metal ions such as Gd^{3+} for example, will have an even greater effect on shortening T1sat, and therefore are unsuitable for producing MT-based contrast, even at very low concentrations.

Experiment 13

[0075] Experiment thirteen was conducted to examine the effect of pH on MT obtained using the lanthanide-macrocylic complexes of the present invention containing two exchangeable sites with different pH responses. Such complexes, for example

$Eu(2)^-$ and $Yb(9)^{3+}$, may be used as pH-reporter-CAs in biological applications.

[0076] The pH dependence of MT obtained for an aqueous solution containing 30 mM $Yb(9)^{3+}$ at 25°C, is shown in FIGURE 28. The saturating RF pulse was applied at the MR frequency of the amide protons (M_{on}), as described in Experiment 11, using either a bandwidth of 600 Hz when H_a and H_b were saturated individually (pwwet = 7.5 ms and wetpwr = 20 db), or a bandwidth of 1500 Hz when for saturating both amide protons simultaneously. Analogous data was collected with the same type of saturating pulse, but located on the opposite side and equal distance away from the bulk water MR signal (M_{off}). The symbols , Δ and O represent data points for saturating H_a, H_b and both sites, respectively. Similar to that observed for $Eu(2)^-$, the relationship between pH and the extent of MT (M_{on}/M_{off}) is complex showing a minimum in MT at about pH 7.4. The same data, expressed as ratios of MT (MTR), are presented in FIGURE 29. MTR is defined as $[1-M_{off}/M_{on}]_{site1}/[1-M_{off}/M_{on}]_{site2}$, where site 1 and site 2 refers to saturation applied to amide protons H_a or H_b or both sites, as indicated in the figure legend. To a first approximation MTR, is proportional to $[\tau_M]_{sites2}/[\tau_M]_{sites1}$. As illustrated in FIGURE 29, MTR increases as a function of increasing pH.

[0077] FIGURE 30 illustrates the effect of pH on MT images obtained while saturating the bound water of the $Eu(2)^-$ complex

(62.5 mM) at 57 ppm, at pH 7.4 and pH 7.8, respectively. These data also illustrate that the NMR signal from the ligand, for example at about 21 ppm, are clearly visible and therefore may be used to determine the concentration of CA agent present in a sample. Because the lanthanide-macrocylic complexes of the present invention contain MR proton signals outside of the frequency range normally observed for biological molecules, it is possible to determine the concentration of such CAs in biological samples by measuring their ^{1}H NMR spectra. It follows therefore, that by measuring the CA's concentration, environmental parameters, such as pH, may be determined by analyzing MT image intensities and applying MT theory, as presented in equations 1 and 2, for example. In comparison, the ^{1}H NMR signals from conventional CA, containing Gd^{3+} for example, are not visible and therefore can not be used as concentration markers.

Experiment 14

[0078] In Experiment 14 several other lanthanide-macrocylic complexes of the present invention were synthesized. For example, a lanthanide-macrocylic complex of the present invention was prepared having the general formula, $Ln(\mathbf{3})^{3+}$, where the four pendent arms R, R', R'' and R''' are all phosphonate diethyl ester-acetamidoacetate (*i.e.*, $LnDOTA\text{-}4AmPE^{3+}$), as depicted below:

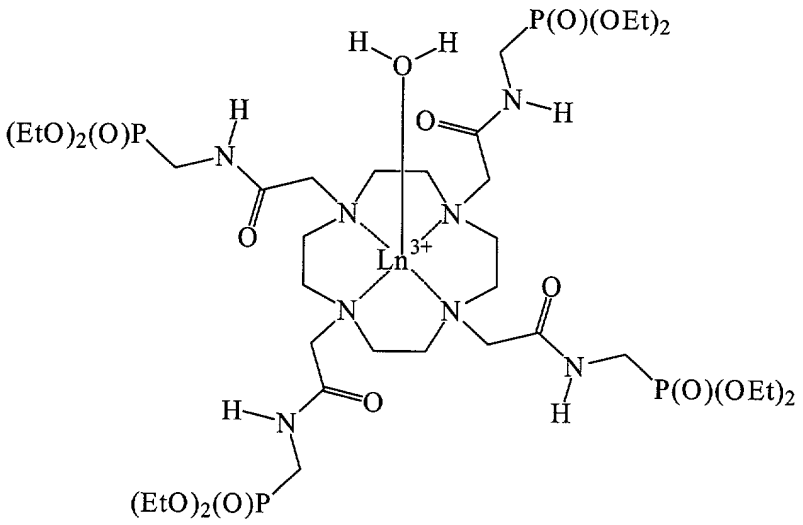

[0079] Another lanthanide-macrocylic complex of the present invention was prepared having the general formula, Ln(**4**)$^{5-}$, where the four pendent arms R, R′, R′′ and R′′′ are all phosphonate-acetamidoacetate (*i.e.*, LnDOTA-4AmP^{5-}), as depicted below:

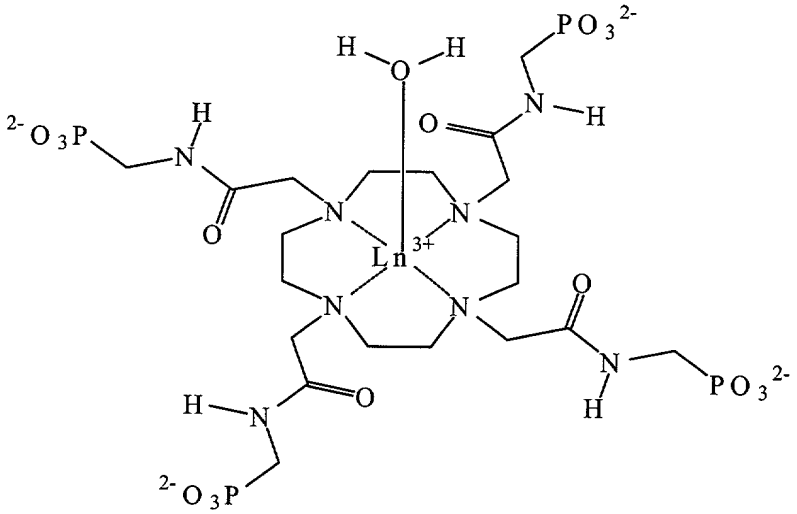

[0080] Yet another lanthanide-macrocylic complex of the present invention was prepared having the general formula, $Ln(\mathbf{5})^{3+}$, where the four pendent arms R, R′, R′′ and R′′′ are all pyridine-acetamidoacetate (*i.e.*, $LnDOTA\text{-}4AmPy^{3+}$), as depicted below:

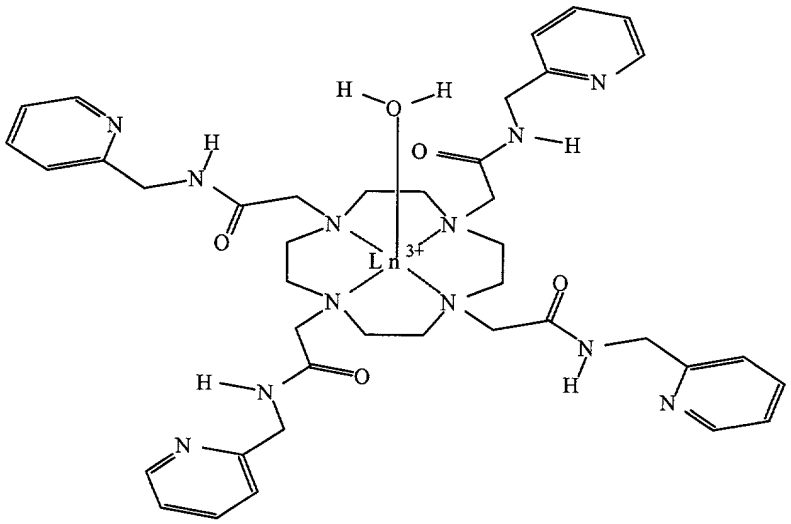

[0081] Still another lanthanide-macrocylic complex of the present invention was prepared having the general formula, $Ln(\mathbf{6})^{3+}$, where the four pendent arms R, R′, R′′ and R′′′ are all phenol-acetamidoacetate (*i.e.*, $LnDOTA\text{-}4AmPhOH^{3+}$), as depicted below:

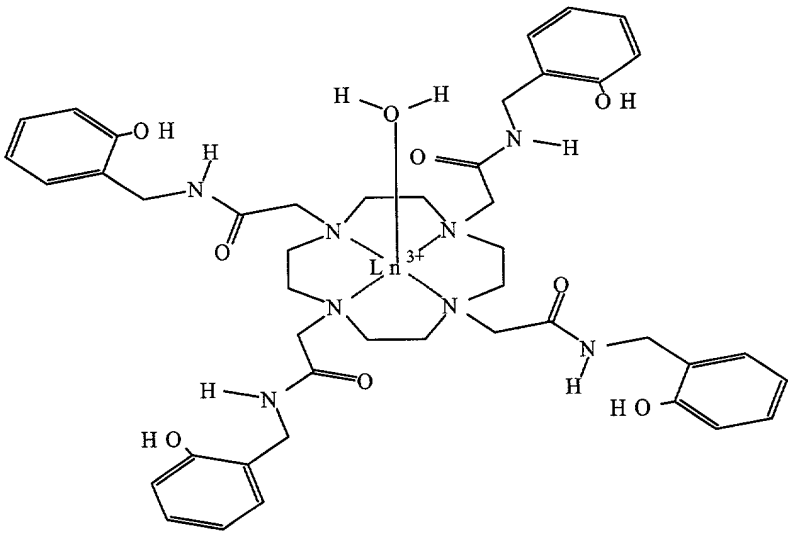

[0082] Another lanthanide-macrocylic complex of the present invention was prepared having the general formula, $Ln(7)^{3+}$, where the two pendent arms R′ and R′′′ are phosphonate diethyl ester-acetamidoacetate and the other two pendent arms R and , R′′ are carboxyethyl-acetamidoacetate (*i.e.*, $LnDOTA\text{-}2AmCE\text{-}2AmPE^{3+}$), as depicted below:

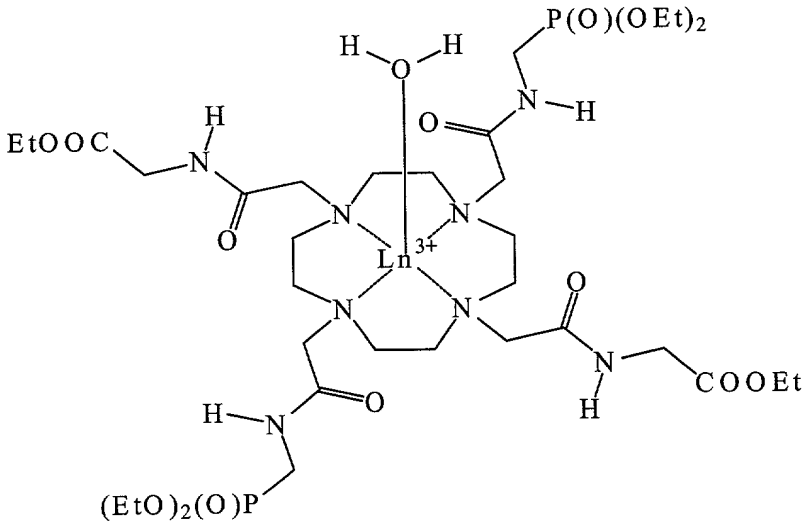

[0083] Another lanthanide-macrocylic complex of the present invention was prepared having the general formula, $Ln(\mathbf{8})^{3-}$, where the two pendent arms R′ and R′′′ are phosphonate-acetamidoacetate and the other two pendent arms R and , R′′ are carboxyl-acetamidoacetate (*i.e.*, LnDOTA-2AmC-2AmP^{3-}), as depicted below:

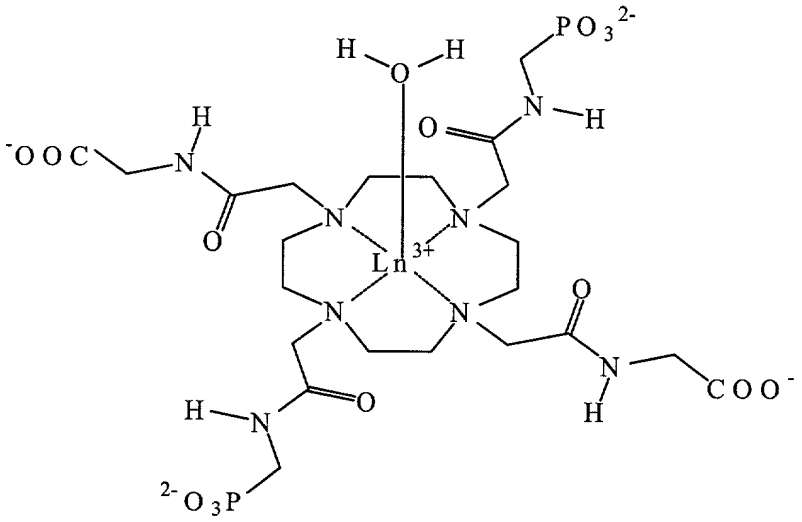

[0084] Although the present invention has been described in detail, those skilled in the art should understand that they can make various changes, substitutions and alterations herein without departing from the spirit and scope of the invention in its broadest form.